american physiological society

JNP JOURNAL OF NEUROPHYSIOLOGY

J Neurophysiol 132: 389–402, 2024.
First published June 12, 2024; doi:10.1152/jn.00370.2023

RESEARCH ARTICLE

Sensory Processing

The precision of signals encoding active self-movement

Joshua D. Haynes,[1] Maria Gallagher,[2] John F. Culling,[1] and Tom C. A. Freeman[1]

[1]*School of Psychology, Cardiff University, Cardiff, United Kingdom and* [2]*School of Psychology, University of Kent, Canterbury, United Kingdom*

Abstract

Everyday actions like moving the head, walking around, and grasping objects are typically self-controlled. This presents a problem when studying the signals encoding such actions because active self-movement is difficult to control experimentally. Available techniques demand repeatable trials, but each action is unique, making it difficult to measure fundamental properties like psychophysical thresholds. We present a novel paradigm that recovers both precision and bias of self-movement signals with minimal constraint on the participant. The paradigm relies on linking image motion to previous self-movement, and two experimental phases to extract the signal encoding the latter. The paradigm takes care of a hidden source of external noise not previously accounted for in techniques that link display motion to self-movement in real time (e.g., virtual reality). We use head rotations as an example of self-movement, and show that the precision of the signals encoding head movement depends on whether they are being used to judge visual motion or auditory motion. We find that perceived motion is slowed during head movement in both cases. The "nonimage" signals encoding active head rotation (motor commands, proprioception, and vestibular cues) are therefore biased toward lower speeds and/or displacements. In a second experiment, we trained participants to rotate their heads at different rates and found that the imprecision of the head rotation signal rises proportionally with head speed (Weber's law). We discuss the findings in terms of the different motion cues used by vision and hearing, and the implications they have for Bayesian models of motion perception.

NEW & NOTEWORTHY We present a psychophysical technique for measuring the precision of signals encoding active self-movements. Using head movements, we show that *1*) precision is greater when active head rotation is performed using visual comparison stimuli versus auditory; *2*) precision decreases with head speed (Weber's law); *3*) perceived speed is lower during head rotation. The findings may reflect the steps needed to convert different cues into common units, and challenge standard Bayesian models of motion perception.

head movement; motion psychophysics; self-movement; vestibular; Weber's law

INTRODUCTION

Bodily movement is a key part of everyday life. Our eyes, head, limbs, and torso are seldom at rest. Action therefore sets the backdrop in which perceptual systems normally operate, with many everyday tasks relying on information about current self-movement. This is derived from a number of perceptual signals, some based on images such as retinal flow, and some based on nonimage sources including the vestibular and motor systems. Information from nonimage sources also plays a role in interpreting images, allowing the observer to differentiate between self-generated movement and movements of external objects.

Success in these active tasks is constrained by two fundamental types of error, namely the precision and accuracy of the underlying perceptual signals. Precision is driven by internal and external noise and corresponds to the width of the distribution of the underlying perceptual signal as it varies across time. Accuracy, on the other hand, corresponds to the distribution's average and is usually referred to as bias. Although a lot is known about the precision and accuracy of image signals, especially in vision and hearing, much less is known about the errors accompanying nonimage signals. This is especially the case when the self-movement is "active" (i.e., self-controlled), partly because it is difficult to apply standard psychophysical techniques to spontaneous actions

Correspondence: T. C. A. Freeman (freemant@cardiff.ac.uk).
Submitted 6 October 2023 / Revised 7 June 2024 / Accepted 7 June 2024

that are under participant control. We therefore developed a new way to measure precision in these circumstances, using head rotation as an example of self-movement. The technique makes no attempt to differentiate between the various sources of nonimage information that are used to encode active self-movement. Rather, it assumes that they are combined to provide a single nonimage signal, and it is the precision of this composite signal that we measure (see Ref. 1 for an example nonimage signal comprising vestibular cues to passive translation and extraretinal cues to eye rotation, and Ref. 2 for an example nonimage signal comprising vestibular and extraretinal cues used to update spatial localization after self-movement). Our technique relies on using image signals as a comparison,[1] which allowed us to compare the results when using vision or hearing in *experiment 1*. We used the same technique in *experiment 2* to investigate whether nonimage precision obeys Weber's law, that is, whether precision scales with magnitude. Investigating Weber's law also allowed us to compare the precision of image and nonimage signals for the stimuli we used.

In a typical precision-measuring task, participants are asked to compare a fixed standard stimulus with a range of test stimuli shown over a series of trials (4–6). The values assigned to the test are usually controlled by a method of constant stimuli or a staircase procedure, both of which provide a measure of a just-noticeable-difference that can be used to estimate the precision of the underlying signal. Crucially, these methods rely on the ability to repeat a set of stimuli over trials. Self-controlled self-movements, however, are not repeatable: every instance of every action is unique. To measure nonimage signal precision, this variability must be accounted for, both within and across trials.

One solution is to use "passive" self-movement because the action is then controlled by the experimenter. The best-known examples come from vestibular research, where participants are moved on a chair or platform (7). Notable examples also come from studies of perceived stability during eye movement, where various contraptions and implements have been used to passively rotate the eye (8, 9). But active nonimage signals also include efferent sources, such as copies of motor commands (10), not just the vestibular, somatosensory and, in the case of passive rotation of the eye, the proprioceptive cues that passive stimulation generates (11–14). Passive stimulation therefore excludes important nonimage sources of self-movement information. Passive stimulation therefore excludes important nonimage sources of self-movement information and is known to give rise to different activity in some neurons within the vestibular nucleus (for a review, see Ref. 15).

Instead, we focus on active self-movement, specifically head rotation, where nonimage sources consist of vestibular cues, motor commands, and proprioceptive feedback, plus any number of somatosensory cues, such as the gliding of hair across the back of the neck. Image-based cues to self-movement were excluded by carrying out the experiments in a completely dark and quiet room, removing important reafferent cues such as retinal flow (16–19). Our method for measuring nonimage signal precision uses two experimental phases, combined with a novel analysis that accounts for the variability of self-movement across trials. The paradigm is sketched in Fig. 1. Based on two-interval forced-choice, the participant makes self-controlled left and right head rotations in the first interval of each trial of *phase 1*, and an auditory or visual stimulus appears in the third sweep (see Fig. 1, *bottom left*). This stimulus is head-centered, because it moves with the participant. The participant is instructed to judge the movement of the stimulus and hence the head movement that drives it. We refer to this interval as the "standard." In the second "test" interval of *phase 1*, shown in the second column of Fig. 1, an auditory or visual stimulus is again shown, but this time with the participant's head stationary. The stimuli move with a trajectory defined by the head movement recorded in the standard interval, but scaled up or down by a multiplicative factor we call "motion gain." Hence, the pattern and duration of stimulus movement experienced in the two intervals is the same, apart from overall magnitude, and is provided by different motion cues. In the head stationary interval, the motion cues depend on image signals. In the head-moving interval, they depend on nonimage signals, including any extraretinal contributions related to smooth compensatory eye movements like the vestibulo-ocular reflex (20), or an inhibitory pursuit drive made to keep the eye head-centered (21). We note that the auditory and visual stimuli used to mark the third head sweep do not provide any informative motion cue per se because they are head-fixed and presented in a dark and quiet laboratory. This remains the case even if their perceived positions shift due to audiogyral (22) and oculogyral illusions (23), which in any case is doubtful given that illusory shifts in position occur over much larger time scales than used in our experiments (24).

Following the two intervals, participants indicate which interval appears to "move more." We avoided the terminology "faster" or "further" because cue preference depends on modality: for vision, participants prefer speed rather than displacement or duration (25, 26), whereas for hearing the reverse is true (27, 28). Motion gain is manipulated across trials using a Method of Constant Stimuli, resulting in a psychometric function that includes two sources of internal noise, one based on the image signal (e.g., visual or auditory motion) and one based on the nonimage signal. To tease these two sources of noise apart, *phase 2*, shown in the third and fourth columns of Fig. 1, isolates the internal noise of the image signal, using the same set of head movement recordings from *phase 1* to move the stimuli in the same trial-by-trial order, but with the head always stationary. Again, the second interval is a scaled version of the first. The precision of the nonimage head rotation signal can then be recovered from *phase 1* as described in METHODS, because image signal precision is now known. We assume that the noise associated with the head-centered auditory or visual target is negligible in the first interval, given that the image is not moving. In comparison, the active self-movement will typically be fast-paced, yielding high levels of internal noise in the nonimage signal.

[1]The term "image" is less intuitive for hearing because space must be recovered indirectly from binaural and monaural cues. Nevertheless, its use is not without precedence [e.g., Middlebrooks and Green (3)]. Here we use it to define the dynamic spatial cues the auditory system uses to recover source movement with respect to the head.

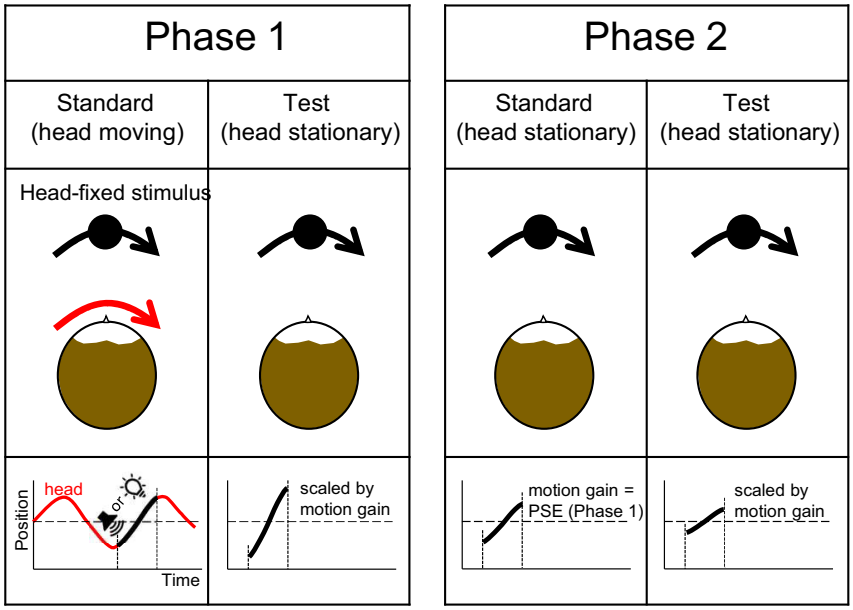

Figure 1. Schematic of the two-phase procedure for measuring the precision of nonimage signals encoding active self-movement. We use head rotation as an example. *Phase 1* consists of two intervals: a standard interval, in which the head moves, and a head-fixed stimulus (visual or auditory) appears "on the nose" in the third sweep; and a test interval, in which the same movement of the stimulus, scaled by the motion gain, is replayed but with head stationary. *Phase 2* also consists of two intervals, both with the head stationary. Here, the motion gain used to scale stimulus motion in the standard interval is set to the Point of Subjective Equality found in *phase 1*. For both phases, a Method of Constant stimuli is used to manipulate motion gain across trials and construct psychometric functions. These are then used to determine the precision of the image signal in the head-stationary intervals, and the nonimage signal in the head-moving interval, based on a model described in the APPENDIX.

In *experiment 1*, we used this novel technique to measure nonimage precision accompanying head rotation, using either auditory or visual stimuli. The modality used to deliver image motion should not affect the measured precision of the nonimage signal because the same image signal (with the same underlying noise) is present in all intervals apart from the first standard interval of *phase 1*. In *experiment 2*, we used auditory stimuli to investigate whether the precision of the nonimage signal obeys Weber's law (i.e., scales with magnitude). The technique requires that eye movements are similar (but not necessarily absent) in the three head-stationary intervals. If this were not the case, then *phase 2* could not be used to estimate the precision of the image signal in the head-stationary test interval of *phase 1*. This was tested in *experiment 2*.

Phase 1 also provides information about bias, specifically whether the magnitude of perceived motion is the same for image and nonimage signals. This is interesting in its own right, partly because it is well known that objects pursued by an eye movement appear slower (29, 30). In this case, the nonimage "extraretinal" signal evidently provides a lower estimate of speed than the image signal. Analogous perceptual slowing has been demonstrated for stimulation of the vestibular system using passive head rotation (31) and active touch (32). It has also been implicated for the auditory system, based on the finding that compensation for head-movement when judging sound-source stability is incomplete (33). But as far as we are aware, whether active head rotation produces the same slowing is currently not known for either vision or hearing.

METHODS

Participants

All observers gave written informed consent, and the experimental procedures were approved by the School of Psychology, Cardiff University Ethics Committee (EC.12.04.03.3123GRA2). In *experiment 1*, five participants took part in the experiment (2 females, 3 males). Two were naïve to the purposes of the experiment and three were experimenters. Participants wore spectacle correction if required. In *experiment 2*, three experimenters and seven participants studying psychology at Cardiff University took part (2 males, 8 females). Only the experimenters were aware of the aims of the experiment. Participants completed at least two replications of *experiment 2*, with eight participants completing three. Eye movements were recorded for nine of the participants. One of these normally wore spectacles, which were removed to allow the eye tracker to operate.

Experiment 1

Stimuli and materials.

Auditory stimuli were played over a 2.4-m diameter ring of 48 Cambridge Audio Minx speakers as shown in Fig. 2. The room was sound treated using wall and ceiling tiles with absorption coefficients of 0.9, and carpet on the floors,

Figure 2. Laboratory setup.

yielding a reverberation time of approximately 60 ms. Data collection was also carried out in complete darkness. The speakers were controlled by two MoTU 24-channel sound cards, each linked to four six-channel Auna amplifiers. Intensity was normalized across individual speakers. The stimuli consisted of white noise spatially windowed by a Gaussian distribution ($\sigma = 5.25^\circ$ in power, equivalent to 0.7 of the speaker spacing i.e., $\sigma = 7.5^\circ$ in amplitude). We have previously shown that this value avoids aliasing artifacts in our speaker system that could occur if the Gaussian distribution is undersampled, while at the same time avoiding the sound becoming too diffuse (34). The noise was sampled at a rate of 48 kHz with a peak level of 70 dB. The position of the spatial Gaussian was refreshed at a rate of 240 Hz, a rate set by the motion tracker described in the section *Head tracking* below. The result was a "blob" of noise that could be moved smoothly across the speakers. The actual motion path taken was determined by the measured head movements, using the motion gain parameter to scale its magnitude.

Visual stimuli were presented to the participant using an AdaFruit NeoPixel strip of 342 LEDs driven by a single Arduino Uno microcontroller. The LED strip was positioned just below the speakers, as shown in Fig. 2, and was driven at a frame rate of 40 Hz. The strip subtended 128° either side of straight ahead. This yielded an LED spacing of 0.75°. To ensure that the LEDs presented stimuli at a comfortable brightness, a single layer of 1.2f neutral density filter reduced the intensity of the display. As with the auditory stimuli, smoothly moving stimuli were created by using a Gaussian distribution that spatially windowed the LED output for each display frame ($\sigma = 1.05^\circ$). To prevent individual LEDs being visually resolved, the strip was placed in a curved enclosure with one open side that was covered by three layers of diffuser gel at a distance of 35 mm, blurring the image. The overall size of the resulting blob was increased slightly by the diffuser ($\sigma = 1.07^\circ$), which we confirmed using a Minolta LS100 photometer and an array of small apertures. The peak luminance of the blob was ~0.042 cd/m^2.

Head tracking.

Head movement was measured using a Polhemus Liberty tracker that sampled position at a rate of 240 Hz. The tracker was mounted to a head band worn by the participant. For the head-moving standard interval of *phase 1*, the head-tracking data were used to detect the third sweep in real-time and keep the subsequent auditory or visual stimulus head-centered (i.e., motion gain = 1). To detect a change in head-movement direction, we convolved the head tracker samples with a finite difference filter to obtain a smoothed derivative. The filter was 13 samples long, meaning there was a 7-frame delay in detecting the head-turn (~30 ms). An example waveform is shown in Fig. 3*A*, with the detected third sweep shown in black and blue.

Procedure.

In *phase 1*, each trial consisted of a "head-moving" standard followed by a "head-stationary" test. The start of the first interval was signaled by a short beep (0.25 s) followed by momentary pause to check the head was centered before the experiment moved on. "Centered" was defined as 10 consecutive head-tracker samples within ±7.5° of the center of the LED/speaker array. Participants were then instructed to move their heads smoothly left and right, or vice versa, at a pace and amplitude that they felt comfortable with. Although it was their free choice, we found some participants alternated the start direction from trial to trial, whereas others mostly started in the same direction. The auditory or visual stimulus appeared during the third sweep and moved with the head. Participants were instructed to fixate it. The start of the second head-stationary test interval was signaled using a blue blob that appeared for 0.2 s, with progress again paused to check the head was centered. Note that the motion in the test interval was based on the third sweep recorded in the standard interval only: the dead-time created by the initial two sweeps was skipped. Unlike the head-moving interval, participants were instructed not to track the stimulus with their eyes but instead keep looking straight ahead. In *phase 2*, the same beep and light were used to identify the start of each interval, with both intervals head-stationary and the initial two sweeps skipped. Each replication of *phase 1* and *phase 2* contained the same number of trials, based on the same head movement recordings, shown in the same order.

Psychometric functions were collected based on a Method of Constant Stimuli using 11 motion gain values. For *phase 1*, these ranged from 0.2 to 1.2 in steps of 0.1 for the auditory condition, and 0.4 to 1.0 in 0.06 steps for the visual condition. The ranges were based on pilot experiments that showed the visual condition produced steeper psychometric functions than the auditory condition. Each motion gain was repeated 10 times, yielding 110 trials per session. For *phase 2*, the same step sizes were used, but the range was

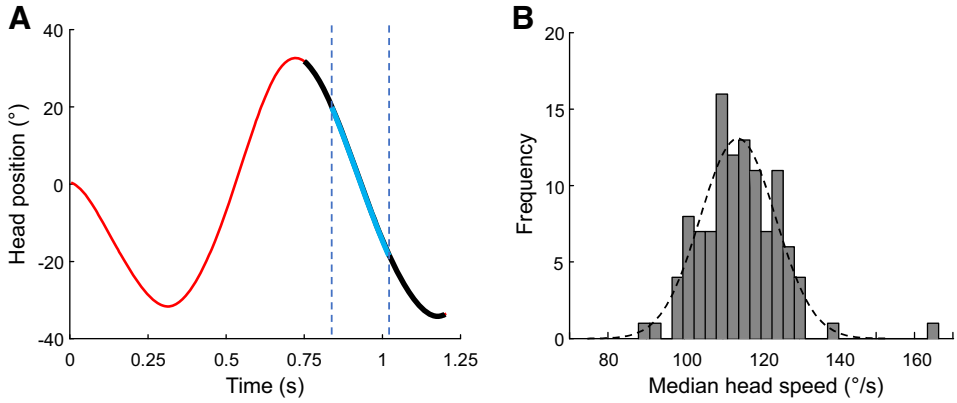

Figure 3. *A*: example head movement waveform. The black portion corresponds to the third sweep as detected by the algorithm described in the text. The visual or auditory stimulus appeared during this time. The blue portion defines the region of interest over which median head speed was calculated for analysis. *B*: an example distribution of median head speeds for a single repetition of *phase 1* (110 trials) for one participant. The dotted line shows the best fitting Gaussian, which was used to determine the mean and standard deviation of the distribution.

centered on the Point of Subjective Equality (PSE) calculated from *phase 1*. This ensured that the precision of the image-motion signal we estimated for each replication of *phase 1* and *2* were based on motion gains centered on a comparable value. The PSE was derived by fitting a cumulative Gaussian to the data using the PAL_PFML_Fit function from the Palamedes toolbox (35), with a lapse rate parameter fixed to 0.02 (note the bespoke psychometric function described in the APPENDIX returns the same PSE as the toolbox).

Participants sat in the center of the speaker/LED ring and wore the head tracking equipment (in *experiment 2* they also wore an eye tracker). Head position was checked with a laser crosshair mounted above the center of the ring, which enabled the participant's midline and interaural axis to be aligned with the speaker ring. The head tracker was boresighted with the participant facing forward and pointing their head toward the central speaker. Boresighting was repeated at the start of each replication of each phase of the experiment.

Each participant repeated three pairs of *phases 1* and *2* for each modality. Psychometric functions were fit to each replication separately. Three of five participants carried out the auditory condition first.

Head movement analysis.

To analyze the head movements after data collection, position samples were first smoothed using MatLab's "low-pass" function with a passband of 8 Hz. The temporal derivative was then taken and the median velocity calculated over a portion of the third sweep that ranged from 20% to 60% of the sweep length (shown in blue in the example waveform of Fig. 3*A*). This region-of-interest (ROI) was adopted because it maximized the number of head-movement samples and goodness-of-fit of the psychometric function (see APPENDIX for evaluation). Figure 3*B* shows an example for one participant of the distribution of these median velocities for one run of *phase 1*. For modeling purposes, the distribution of each 110-trial run was fit with a Gaussian (dotted line in Fig. 3*B*) to extract a mean and standard deviation.

Psychophysical analysis.

The distribution shown in Fig. 3*B* emphasizes the fact that, as with other self-movements, head rotation varies across trials. Using motion gain therefore seems to be a good way of controlling for this variability because it directly links image motion to the ongoing self-movement in real-time. The patterns of motion are therefore identical, meaning the only difference between signal inputs is speed and displacement—duration is fixed. On the face of it, therefore, motion gain provides the experimenter with a repeatable parameter that can be used to define a psychometric function or drive a staircase. Examples are provided by Serafin et al. (36) and Steinicke et al. (37), who plot psychometric functions defined by changes in motion gain within acoustic and visual virtual reality setups, respectively. However, closer inspection of their figures suggests a consistent feature not accounted for by fitting a standard cumulative Gaussian: on occasions, their data appear to asymptote more than a constrained lapse rate parameter would allow [e.g., <6%, as suggested by Wichmann and Hill (38)]. In the APPENDIX, we construct a model of the psychophysical task that shows why. The model emphasizes that motion gain is not always a good shorthand for the actual stimulation experienced by the participant, namely the magnitude of motion (speed or displacement).

In keeping with standard signal detection theory, the model assumes that participants base their judgment on a point estimate of stimulus magnitude (e.g., the peak speed of head and image movement, or average speed, or displacement). Crucially, in addition to internal noise, the point estimates vary across trials due to the external noise introduced by variable self-movement. The external noise produces some surprising effects (see Fig. A1). First, the function's true slope is steeper than the best-fitting single cumulative Gaussian. Second, as the variability of the self-movement increases, the function's asymptotes depart markedly from 0 and 100%, much further than a typical constrained lapse rate parameter of 6% would allow.

Following standard practice, we assume that internal and external noise is Gaussian distributed. The precision of a given signal is therefore defined by its standard deviation. If the self-movement did not vary at all, the precision of the nonimage signal could be calculated by standard fitting of a cumulative Gaussian to the psychophysical data, and then applying the "variances sum" law to both phases. Thus, for *phase 1*, $\sigma^2_{G_1} = \sigma^2_i + \sigma^2_h$, where the subscripts correspond to the cumulative Gaussian fit to the data (G_1), the image signal (auditory or visual, i), and the nonimage signal encoding head rotation (h). For *phase 2*, $\sigma^2_{G_2} = 2\sigma^2_i$; hence the precision of the nonimage signal (σ^2_h) in *phase 1* can be found by substitution. But, when self-movement varies, this standard approach is an approximation at best. Variable self-movement adds external noise that varies across the psychometric function because it is scaled by motion gain; hence the assumption of a single cumulative Gaussian is not correct. We develop the appropriate formulae in the APPENDIX and show how these can be used to extract the internal noise of the image signal (σ^2_i) and nonimage signal (σ^2_h) from the two phases of our experiment. Similar formulae can be applied to a more typical motion gain scenario used in virtual reality setups, where both self-movement and image motion are shown at the same time (36, 37, 39–41).

Experiment 2

Stimuli and procedure.

The aim of *experiment 2* was to determine signal precision as a function of head and stimulus speed. Before each replication of the main experiment, a training session was therefore run to help participants rotate their heads at one of the five target speeds. The training stimuli were audiovisual, consisting of visual and auditory blobs as used in *experiment 1*. These moved in synchrony. The procedure for the main experiment was the same as *experiment 1*, consisting of two experimental phases linked by the set of head movements recorded in the first. Unlike *experiment 1*, only auditory stimuli were used. Each trained head speed was investigated by completing training and main experiment data collection in pairs. This process was repeated three times, yielding 15 training and main experiment pairs, presented in a random order.

Head speed training sessions.

Training sessions consisted of a two-stage process that was run ahead of each replication of the main experiment. In *stage 1*, participants were asked to track an audiovisual stimulus with their head. The stimulus moved independently along a sinusoidal path at a frequency of 1 Hz at one of five amplitudes: 5°, 12.5°, 20°, 27.5°, 35°. These correspond to median target speeds from 30.0°/s to 209°/s for the ROI defined in *experiment 1*. Five and three-quarter periods were shown for each speed to generate 12 sweeps. In *stage 2*, participants attempted to reproduce the trained head speed, this time using a head-stationary audiovisual fixation target moving with the nose as a guide (motion gain = 1). Again, they completed 12 sweeps, determined by recording the number of head direction reversals detected in the head tracking as described in *experiment 1*. The accuracy of head rotation was assessed by calculating the median head speed for each of the final 10 head sweeps as described in *experiment 1*. If seven of 10 sweeps had a median within 5°/s ± 5% of the desired training speed, performance on that training run was deemed sufficiently accurate. If not, the participant was given feedback on how many sweeps were accurate, and how many were too fast and/or slow, and the run repeated. Participants had to complete at least three training runs, with at least one successful run before progressing to each replication of the main experiment.

Eye tracking and analysis.

Eye movements were tracked using a Pupil Labs Pupil Core head-mounted eye tracker. The tracker had a 120 Hz sampling frequency and a front-facing world camera. The camera was used for calibration by having participants look at a 3 by 2 array of calibration points that can be seen in Fig. 2. These were used to convert the eye tracker's normalized units into degrees. To analyze, samples with less than 0.6 confidence as defined by the Pupil Labs software were excluded, and the gaps filled using linear interpolation (41). Gaps were more frequent for the head-moving condition. If the number of dropped samples was 50% or greater, the waveform for that interval was excluded from the analysis.

The remaining waveforms were smoothed using a Gaussian filter ($\sigma = 16$ Hz in the frequency domain). The first, second, and third derivatives were then taken numerically, corresponding respectively to velocity, acceleration, and jerk. Saccades were detected using Wyatt's jerk analysis, with a jerk threshold set to 2×10^5°/s^3 (42). Saccadic samples were removed from the analysis, along with four samples either side of each detected saccade, plus the initial 20 samples at the start and end of each waveform. Mean velocity and speed were then calculated for the third sweep for each head-movement interval, and the single sweep in each head-stationary interval. For comparison, the vestibulo-ocular reflex (VOR) needed to maintain stable fixation on a world-stationary point at the same distance as the speakers was calculated, using the approximation described by Leigh and Zee (43, p. 274): $E = -H(1 + R/D)$, where H is the head velocity, $R = 0.1$ m (the approximate distance from the eye to center of head rotation) and $D = 1.2$ m (the distance from participant to speakers). Note that we assume the eyes were fixating at this distance because a visible fixation point appeared there before the second interval of each trial (for details, see *Procedure* section above).

RESULTS

Experiment 1: Precision of Signals Encoding Active Head Rotation

Figure 4*A* shows the mean precision of the nonimage head-rotation signal (bars) across the five participants together with their individual data (solid points). Nonimage signals were less precise in the auditory condition, producing a significant increase in the standard deviation of the underlying signal distribution as defined by the model described in the APPENDIX [$t(4) = 4.19$, $P = 0.01$]. Contrary to our prediction, therefore, modality appears to matter. Figure 4*B* shows that head speeds were slightly faster on average when an auditory target appeared in the third head sweep compared with a visual one, however this difference was nonsignificant [$t(4) = 1.76$, $P = 0.15$]. We note that this lack of effect may have been driven by the participant shown with closed circles, who, unlike the other participants, did not show any decrease in mean head speed in the visual condition. It remains possible, therefore, that the difference in nonimage signal precision could be explained in part by a scaling of precision with magnitude (i.e., Weber's law). This point is explored further in *experiment 2*, where Weber's Law was investigated more thoroughly.

Figure 5 shows the mean PSEs obtained from *phase 1*. The PSEs are similar for vision and hearing [$t(4) = -0.71$, $P = 0.52$]. The PSEs are around 0.7, meaning that stimuli had to be slowed by 30% when they moved passed a stationary participant to achieve a perceived speed match with head moving interval. For vision, this finding resembles the Aubert–

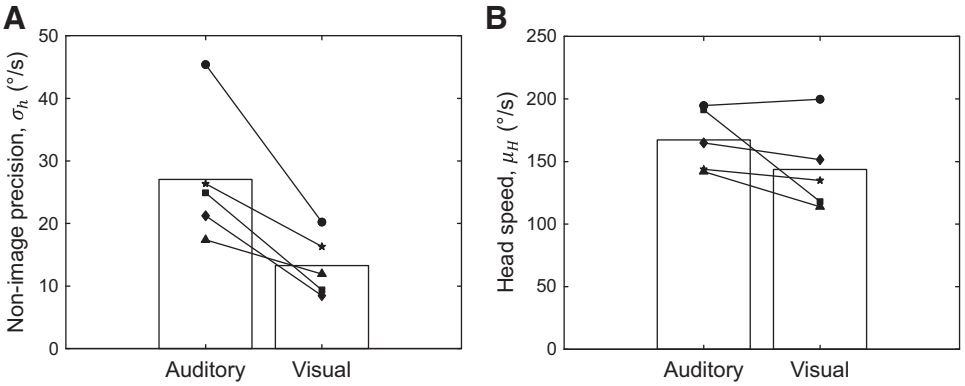

Figure 4. *A*: precision of the nonimage signal encoding head rotation for the two stimulus conditions. Precision is defined as the standard deviation of the underlying signal distribution, determined by the model in the APPENDIX. Note therefore that larger standard deviations correspond to the less precise signals. Bars correspond to the mean of the individual data points, with the latter shown as solid symbols. *B*: head speed using the same format.

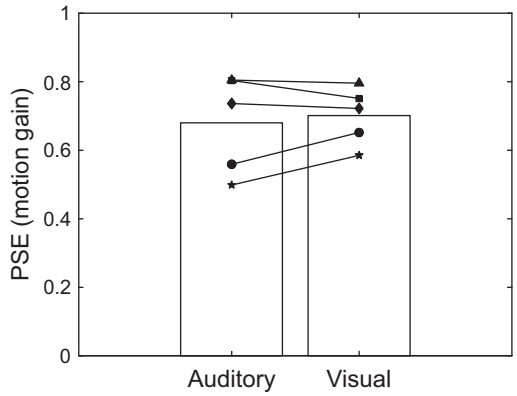

Figure 5. Point of Subjective Equalities (PSEs) for the psychometric functions collected in *phase 1*. These indicate the relative bias between image and nonimage signals for both modalities. A value less than 1 means that head tracked stimuli appear slower. Bars correspond to the mean of the individual data points, with the latter shown as solid symbols.

Fleischl phenomenon (29, 30), where motion appears slower if stimuli are tracked by a smooth eye pursuit. Our data show that perceived slowing occurs for active head rotation too, albeit for auditory and visual stimuli that are linked directly to the self-movement, as opposed to being pursued in a more typical closed-loop manner. It is also worth noting that the biases we found are comparable with those reported for passive head rotation (31).

Experiment 2: Do Nonimage Signals Obey Weber's Law during Active Head Rotation?

For many sensory systems, discrimination thresholds scale proportionally with stimulus magnitude over a wide range. This is known as Weber's law (44). In *experiment 2*, we investigated the extent to which nonimage signals accompanying active head rotation adhered to Weber's law by training participants to rotate their heads at different speeds. The same two-phase protocol described in *experiment 1* was used to measure nonimage precision at each trained speed, using auditory stimuli only. These data also allowed a more direct comparison between nonimage and image precision. This was not possible in *experiment 1* because the two-phase protocol forces the motion gain of the standard in *phase 1* to be different from that used in *phase 2* (i.e., gain = 1 and PSE, respectively). By manipulating head speed in *experiment 2*, signal precision can be described as a function of magnitude, allowing the comparison to be made.

Figure 6*A* plots the mean head speed made by participants in the main experiment. The dashed line indicates perfect performance with respect to the head speeds they were trained on prior to data collection. Head movements were reasonably accurate in the main experiment, producing a well separated set of rotation speeds that covered a wide range [$F(4,45) = 16.89$, $P < 0.001$].

Figure 6*B* plots the mean eye velocity for 9 of 10 participants whom we were able to obtain recordings for. The dashed line indicates the predicted VOR needed to maintain fixation on a world-stationary point at the same distance as the speakers (see METHODS for details). Figure 6*C* plots the mean speed (i.e., unsigned average). In both cases, there was a significant main effect of interval [eye velocity: $F(3,24) = 23.07$, $P < 0.001$; eye speed: $F(3,24) = 58.5$, $P < 0.001$], and a significant interaction with trained speed [eye velocity: $F(12,96) = 2.32$, $P = 0.012$; eye speed: $F(12,96) = 17.52$, $P < 0.001$]. Simple effects showed that the interaction was driven by the effect of trained speed on eye speed in the head-moving interval [$F(1,4) = 16.98$, $P < 0.001$], with the same simple effect for eye velocity being close to significant [$F(1,4) = 2.38$, $P = 0.073$]. Importantly, however, the eye movement in the head-moving interval was many orders of magnitude smaller than expected from compensatory VOR.

The simple effects for the head-stationary intervals were all nonsignificant ($P > 0.254$ or greater). Post hoc comparisons, collapsed across trained speed, showed that none of the head-stationary intervals were significantly different from each other, confirming a key assumption of the paradigm. All three, however, were significantly different from the head-moving interval (Bonferroni-corrected $P < 0.001$). Whether the relatively small eye movements found in the head-moving interval could explain the differences between modalities found in *experiment 1* is taken up in GENERAL DISCUSSION.

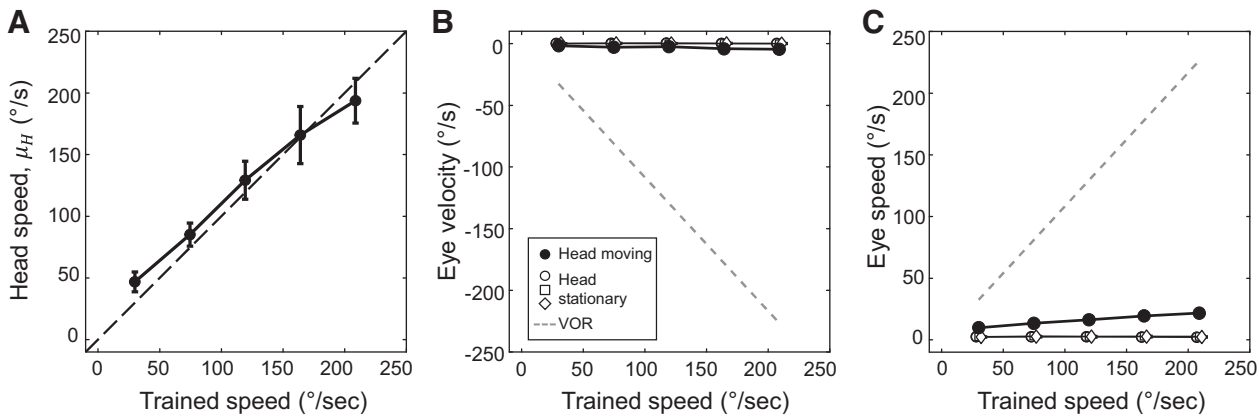

Figure 6. *A*: mean head speed for 10 participants over the region-of-interest (ROI) defined in Fig. 3*A*. The dashed line shows perfect performance with respect to the head speed they were trained on prior to the main experiment. *B*: mean eye velocity over nine participants for the two intervals in each phase. Open symbols correspond to the three head-stationary intervals, with circles used for the one in *phase 1* and open squares and diamonds for two in *phase 2*. Closed circles correspond to the head-moving interval. The dashed line defines the vestibulo-ocular reflex (VOR) needed to maintain stationary gaze on a world-centered point at the same distance as the speakers. Negative values correspond to an eye movement against the head rotation. *C*: mean eye speed (unsigned average). Error bars are ±1SE and can be smaller than symbol size.

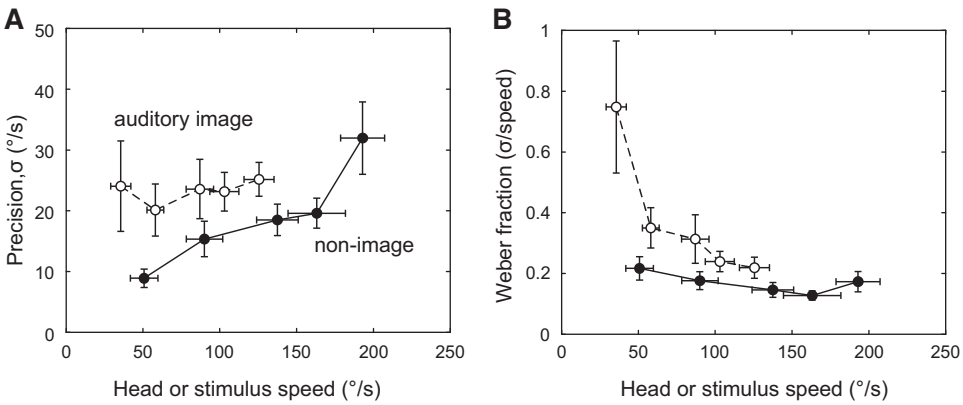

Figure 7. *A*: precision as a function of stimulus speed for the auditory image signal (open symbols) and nonimage signals (closed symbols). Precision is defined as the standard deviation of the underlying signal distribution determined by the model in the APPENDIX. Larger standard deviations correspond to less precise signals. *B*: the same data expressed as Weber fractions (i.e., standard deviation/speed). Error bars are ±1SE.

Figure 7*A* plots the nonimage signal precision (filled circles) and auditory image signal precision (open circles) as a function of the mean head or stimulus speed, respectively. The latter compresses horizontally because the speeds are set by the PSE obtained from *phase 2* of the main experiment. This corresponds to a motion gain of around 0.7 (see Fig. 8 for the PSEs at each training speed). The horizontal compression is therefore around 30% compared with the closed circles.

For the auditory signal, precision did not vary with stimulus speed [$F(4,45) = 0.154$, $P = 0.96$]. However, for the nonimage signal, precision decreased with head speed, such that the standard deviation of the underlying signal distribution significantly increased [$F(4,45) = 6.035$, $P < 0.001$]. Also evident is the fact that the auditory image signal is less precise than the nonimage signal over the range of stimulus speeds tested. Figure 7*B* plots the same data as Weber fractions (i.e., standard deviation divided by head or stimulus speed). For both types of signal, precision adheres to Weber's law for medium to high speeds. Thus, the Weber fractions are approximately constant over much of the range of speeds tested. At lower speeds, however, the two functions differ, with Weber fractions starting to rise steeply for hearing. This rise is reminiscent of other studies of Weber's law in the perception of auditory motion (5). The same is not true for the nonimage signal, where Weber's law appears to hold reasonably well across all head speeds investigated. This finding is similar to previous work using passive stimulation of the vestibular system (4).

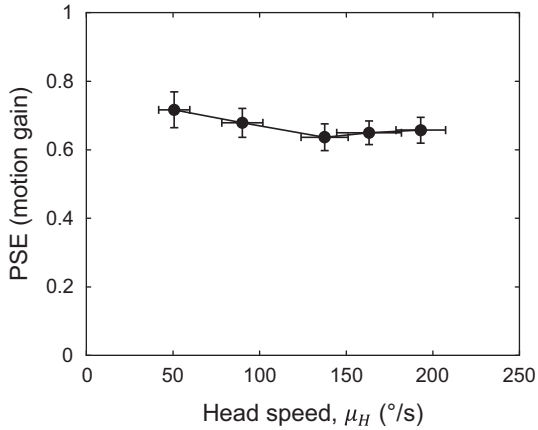

Figure 8. Point of Subjective Equalities (PSEs) from *phase 1* as a function of head speed. Error bars are ±1SE.

Figure 8 plots the mean PSEs from *phase 1* as a function of head speed. They appear similar for all head speeds experienced [$F(4,45) = 0.57$, $P = 0.69$]. Hence, the same proportional reduction in image speed was needed to match the perceived motion in the head movement interval. This value was around 0.7, replicating the findings in *experiment 1*. Over a wide range of head speeds, therefore, moving auditory stimuli appear slower during head movement, akin to the Aubert–Fleischl phenomenon in vision. However, unlike vision and pursuit eye movement (45, 46), the nonimage signal appears more precise than the auditory image signal, which could have important implications for the interpretation of the bias shown in Fig. 8. This point is taken up in more detail in GENERAL DISCUSSION.

In *experiment 1*, we found nonimage signal precision was higher using visual stimuli compared with auditory stimuli. To investigate further, we fit a regression line to the nonimage precisions in Fig. 7*A* using Deming's technique, a procedure that is used when both *X* and *Y* values are dependent measures with error (47). The result is shown in Fig. 9, together with the two nonimage signal precision values found in *experiment 1*. The regression analysis shows good agreement between *experiments 1* and *2* for auditory stimuli. The precision value from *experiment 1* (open circle) falls very close to the regression line determined by *experiment 2*, indicating good replicability of our technique. At the same time, however, the analysis casts further doubt on whether Weber's law can explain the better nonimage signal precision found using visual stimuli (open triangle). If Weber's law were to account for the discrepancy in precision, the head speeds in the visual condition of *experiment 1* would need to be roughly halved to shift the open triangle horizontally onto the regression line. Reasons why modality might affect nonimage signal precision are taken up in GENERAL DISCUSSION.

GENERAL DISCUSSION

We have proposed a novel technique for measuring the combined precision of the nonimage signals that encode active self-movement (e.g., vestibular cues, proprioception, and motor commands). Traditional psychophysical techniques are difficult to use in these situations because spontaneous self-movement is under participant control. Stimulation

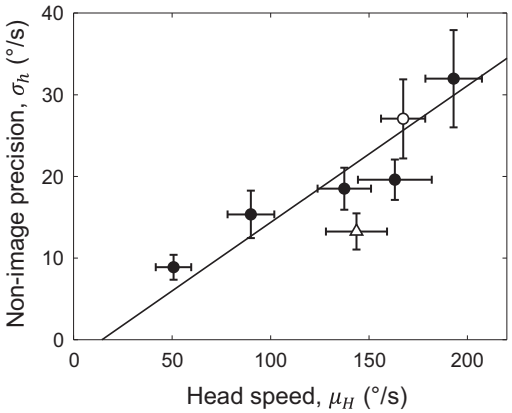

Figure 9. Deming regression (solid line) for the nonimage signal precision data from *experiment 2* (filled circles). The open circle is the nonimage signal precision from the auditory condition of *experiment 1*, and the open triangle the visual condition. Error bars are ±1SE.

is therefore not repeatable across trials. The new technique relies on the following three factors: *1*) linking image motion to prior self-movement using a motion gain parameter that can be manipulated in a consistent fashion across trials; *2*) the generation of two psychometric functions limited by identical sources of noise, apart from the internal noise related to nonimage signals encoding active self-movement; *3*) a model that yields the internal noise sources, while controlling for the external noise created by self-movement as it varies across trials. The technique could easily be adapted for other examples of active self-movement, such as walking and active touch, and situations where nonimage signals and image signals are experienced simultaneously (e.g., virtual reality).

Assumptions of the Model

The model assumes that eye movements made in all head-stationary test intervals are similar. If this were not the case, then the image noise in *phase 2* could be different from the image noise in the test interval of *phase 1*. For instance, if observers pursued the stimuli in the test interval of *phase 1*, but not *phase 2*, then motor cues related to the pursuit system would be present in the first phase but not the second. However, the eye movement recordings in *experiment 2* showed that fixation accuracy was similar in all head-stationary test intervals, with the evidence suggesting that observers were able to keep their eyes stationary. In the head-moving interval, however, we found small eye movements against the head rotation, but these were many orders of magnitude less than would be expected from compensatory VOR. Although we did not measure eye movements in *experiment 1*, it is unlikely that fixation accuracy explains the difference in nonimage precision found when using auditory and visual stimuli. This is because eye fixation would likely be more variable using head-fixed auditory stimuli compared with visual stimuli, and yet fixation accuracy was already very good when using sounds in *experiment 2*.

The model assumes that internal noise is fixed. At first sight, this seems at loggerheads with the findings of *experiment 2*, which show that the precision of the nonimage signal declined as head speed increased. However, although the internal noises were assumed to be fixed across the psychometric function describing each head-speed condition, they were free to vary across conditions. We view the fixed noise assumption as a reasonable approximation for the range of stimuli used to recover a given psychometric function. Indeed, the fixed noise assumption is implicit when fitting a single cumulative Gaussian to the data, unless stimulus values are logged.

The model also assumes that the noise associated with an image signal at rest is negligible. Accordingly, in the head moving interval, the noise that limits performance is assumed to be driven entirely by the nonimage signal. For active self-movement this is a reasonable approximation because the magnitudes are typically high, yielding noise far greater than any other signal at rest. An example is provided by Clemens et al. (1), who made a similar assumption when modeling cue combination between vestibular and extraretinal cues. We note, however, that this approximation is less appealing at slow speeds. A case in point is smooth pursuit, where at least one previous model of perceived speed includes noise terms for the resting state of both retinal and extraretinal signals (45), in part because the speeds considered were relatively slow (2–12°/s).

Measurement Noise

The psychometric functions derived from *phase 1* and *2* are based on the same measurements of head rotation. This controls for any effect of measurement noise introduced by the head tracker because the (head-stationary) test intervals are based on the same set of recordings, presented in identical order. The effect on the precision of the image signal in the two phases is therefore the same, such that any influence is canceled out.

This does not mean that all of our conclusions are therefore immune to the effect of measurement noise. A case in point is the comparison carried out in *experiment 2* because measurement noise could differentially affect the estimates of auditory signal precision, as these estimates are based on one phase only. However, the effect of measurement noise is probably small. We measured the standard deviation of position samples output by our head tracker as ~0.55°. This is considerably lower than the positional noise needed to produce significant changes in speed discrimination thresholds previously reported for visual stimuli (48, 49). For instance, in the "high noise" condition of Bentvelzen et al., positional noise was added to their LED system with a standard deviation of 7.4° and an update rate of 25 Hz. This produced thresholds that doubled compared with baseline. If the stimuli used in *experiment 2* had been visual, we would therefore expect thresholds to change around 7.4% (i.e., 0.55/7.4 × 100%). Bentvelzen et al. used a two-interval technique, so in terms of the precision we report, this equates to a 5.25% change in the standard deviation of the underlying signal. This is a much smaller difference than found between the auditory image signal and nonimage signal in *experiment 2*. Moreover, spatial hearing is considerably less precise than perifoveal vision, suggesting the effect would be smaller still.

Vision versus Hearing

Experiment 1 showed that nonimage signal precision was lower when using visual stimuli than auditory stimuli in the

head-stationary test intervals. We also found that head speeds were slightly lower too, but the suggestion that Weber's law might explain the difference in precision was not supported by the regression analysis of *experiment 2*. Here, we discuss two possible reasons for this difference.

The first concerns extraretinal signals originating from the eye movement system during head movement. These can be produced by both reflexive (20) and deliberate eye movements (e.g., smooth pursuit—for a review, see Ref. 50). They can also arise when compensatory VOR is inhibited to fixate head-stationary targets during head rotation (21). Hence the relationship between extraretinal input and eye movement recordings is not straightforward. Halow et al. (41) make a similar point when trying to account for changes in perceived scene stability during active and passive vestibular stimulation, combined with different fixation strategies including the use of head-fixed targets. Nevertheless, in *experiment 2*, we found that eye movements were small, indicating good adherence to the instruction to fixate the head-dependent sound. We assume that fixation of a head-fixed visual target would have been the same or slightly better (e.g., see Refs. 1 and 41). On this basis, we doubt that extraretinal input could explain the difference, given that the change in nonimage precision was almost a factor of 2 between modalities in *experiment 1*.

A second possible reason for the large difference in nonimage precision that we found is the need to convert perceptual signals into common units. The nonimage signal combines vestibular and motor cues, both of which are likely to be based on speed. In the case of the vestibular system, the canals mechanically integrate rotary acceleration for all but very low rates (51), leading to canal afferents that encode speed (15, 52). In the case of motor signals, Freeman et al. (25) showed that observers prefer speed versus displacement and duration cues when judging the motion of a pursued target, and that the speed cue was based on extraretinal signals (i.e., motor commands and/or proprioception). Assuming the same is true for head rotation, the motor signals in our experiments were also in speed units. Hence, the nonimage signal likely encodes speed, making the comparison with visual motion signals relatively straightforward because vision prefers speed over displacement (25, 26). However, the same cannot be said for hearing, which prefers displacement cues over speed (27, 28). The mismatch for hearing can be resolved by integrating the nonimage signal. A transform like this may add noise, leading to a nonimage signal that is less precise when moving sounds are used.

An alternative, suggested by one of the reviewers, is that "silent" visual and auditory cues to self-movement, such as retinal flow, could have played a part in explaining the difference in precision. The idea is that image-signals related to the background are always on and integrated with other self-movement cues, even though our experiments were carried out in a dark and sound-deadened room. This could lead to apparent differences in estimates of "nonimage" precision, and also perceived motion that is lower during head movement, assuming that these undetectable cues are integrated in the same way that detectable cues to self-movement are (53), and that different undetected cues were used in the two conditions. However, we are not aware of any models of cue combination that include undetected cues. An example would be Hillis et al. (54), who identified three additional cues not included in their model. They resolved this issue like us, by making these cues undetectable in their experiments.

Weber's Law

In *experiment 2*, we found that Weber's law described the precision of both image and nonimage signals for medium to high speeds. However, at low speeds Weber fractions for the auditory image signal rose steeply, unlike those for nonimage signal precision. Both findings echo previous reports in the literature. For auditory motion based on interaural time differences, Altman and Viskov (5) found Weber fractions were roughly constant from around 60–140°/s but rose steeply at lower speeds. For vision, the same rise at slower speeds is found but matched by a similar rise at faster speeds (6). In the case of the nonimage signal, passive vestibular stimulation reveals good adherence to Weber's law similar to the results we found for active self-movement, although further analysis by Mallery et al. (4) showed that a power law with an exponent around 0.4 is better description of the raw thresholds than the straight line predicted by Weber's law. Similar behavior has been reported for the variability in the vestibulo-ocular reflex, an eye movement controlled by the vestibular system (55). One implication is that the nonimage signal we measured is dominated by the vestibular system, despite the fact that some neurons in the vestibular nucleus are suppressed during active self-movement (15). This implication only holds if the precision of motor signals encoding head rotation behave differently to the vestibular signals potentially dominating performance in our experiments, but we are unaware of any studies that have isolated the precision of motor cues.

Bayesian Models of Motion Perception

In both *experiments 1* and *2* we found that perceived speed was lower when the head rotated. The bias was very consistent across modalities (*experiment 1*) and stimulus speed (*experiment 2*), adding to a large body of evidence showing that nonimage signals based on eye rotation, head rotation, and hand/arm movement typically provide lower estimates of motion magnitude than signals encoding image motion in vision, hearing, and touch. On the face of it, the bias between nonimage signals and image signals is puzzling because one might expect this type of constant error to be calibrated out by the perceptual system. One possible explanation is that the bias results from a Bayesian observer balancing unbiased yet imprecise sensory information against prior expectations about the state of the world. The result is a posterior distribution that has greater precision than the original measurements, but not necessarily greater accuracy. As signals become noisier, the position of the posterior is increasingly pulled toward the prior distribution such that accuracy shifts. For motion, the claim is that the prior peaks at 0 because most objects are at rest (56). Hence, as motion signals become noisier, speed estimates reduce.

The Bayesian framework has been used to explain why perceived visual speed slows at low contrast (57), why pursued objects appear slower (45, 46), why moving sounds appear slower when presented against background noise (58), and why tactile stimuli appear slower when made

noisier or "pursued" by an hand/arm movement (32). It can also be used to account for individual differences in motion perception (46). Nevertheless, the overarching theory is not without its detractors (59–61). One simple test is to correlate measures of precision (e.g., thresholds) with bias—the Bayesian hypothesis predicts that as precision declines, perceived speed should slow. Many of the papers cited earlier show this to be case. However, there are a growing number of reports that this is not always true. Some recent studies in vision, hearing, and vestibular research have shown changes in bias with little evidence for changes in precision (31, 33, 60, 62). At least one paper reports the opposite (49). The findings of *experiment 2* seem to add to these "non-Bayesian" set of results. They show that auditory motion signals are less precise than nonimage signals, even though the latter produce substantially lower estimates of motion magnitude.

Conclusions

We have presented a novel technique for the measurement of the precision of nonimage signals encoding active self-movement. We used head rotation as an example of self-movement, and showed that the precision measured was different using auditory and visual stimuli. One possible explanation is that more steps are needed to get nonimage signals and auditory image signals into the same perceptual units. In agreement with current literature, we found that the nonimage signal obeys Weber's law over a wide range of stimulus speeds, unlike its image-based counterpart. We also found that the magnitude of perceived motion is reduced during head movement for both vision and hearing. This finding is difficult to explain within a Bayesian framework because we found that image signal precision was lower than nonimage signal precision over the wide range of stimulus speeds investigated.

APPENDIX

Phase 1 consists of a head-movement interval followed by an image-motion interval. In the first, there is no image motion as the object is spatially linked to the movement of the participant. Perceived motion therefore depends on a point estimate (h) of the nonimage signal encoding head rotation. We assume that h is corrupted by fixed additive Gaussian noise across trials. Using $N(\mu, \sigma)$ to denote a normal distribution with mean μ and standard deviation σ, the nonimage signal is therefore distributed as $h = \mu_h + N(0,\sigma_h)$. The mean μ_h depends on the head movement magnitude (H), which we also assume is normally distributed across trials (see Fig. 3*B* in the main text). Perceived motion in *interval 1* (M_1) is therefore:

$$M_1 = bN(\mu_H, \sigma_H) + N(0, \sigma_h) \quad (A1)$$

where b is a linear bias term that sets the gain of the head-movement signal relative to its input, i.e., $h = bH$. Note that either speed or displacement could be used to characterize the distributions of head rotation and signals (to reiterate a point made in the main text, displacement and speed are perfectly correlated when manipulating motion gain because duration is fixed). The model is ambivalent. Swapping between speed and displacement changes the units but not the relative differences found for a chosen parameter across conditions.

In the second interval, image motion (I) moves as a fixed proportion (g) of the head movements recorded in *interval 1*: $I(t) = gH(t)$. We refer to g as the "motion gain." As the head and eyes are stationary, sensed movement depends on an image signal (i). Following similar logic to *interval 1*, the perceived motion in *interval 2* is therefore:

$$M_2 = gN(\mu_H, \sigma_H) + N(0, \sigma_i) \quad (A2)$$

Note that *Eq. A2* assumes that the image signal is unbiased. Hence b in *Eq. A1* defines the relative bias between h and i, such that $b < 1$ means that the nonimage signal registers a lower magnitude than the image signal. Following standard signal detection theory (e.g., see Ref. 63), we assume observers base their choice on an internal decision variable (d) that depends on the difference between the perceived motion in the two intervals:

$$d = M_2 - M_1 \quad (A3)$$

The choice "*interval 2* appears to move more" corresponds to $d > 0$. From signal detection theory we define

$$d' = \frac{\mu_d}{\sigma_d} \quad (A4)$$

such that the probability of choosing *interval 2* is given by:

$$P = \frac{\lambda}{2} + (1 - \lambda)\Phi\left(\frac{d'}{\sqrt{2}}\right) \quad (A5)$$

where λ is the lapse rate and Φ is the cumulative distribution function of the standard normal distribution.

Substituting *Eqs. A1* and *A2* into *Eq. A3*:

$$d = (g - b)N(\mu_H, \sigma_H) + N(0, \sigma_i) + N(0, \sigma_h) \quad (A6)$$

By inspection:

$$\mu_d = (g - b)\mu_H \quad (A7)$$

Note that the PSE occurs when $\mu_d = 0$. At this point $g = b$; hence the relative bias between h and i can be read directly from the psychometric function. If the bias $b < 1$, then the PSE occurs when image motion is slower than head-movement. This is analogous to the Aubert–Fleischl phenomenon (29, 30), in which moving objects appear slower when pursued. Conversely, if $b > 1$, then image motion must be faster to achieve the PSE.

To obtain σ_d, we sum the variances of the three distributions defined by *Eq. A6* and take their square root:

$$\sigma_d = \sqrt{(g - b)^2\sigma_H^2 + \sigma_h^2 + \sigma_i^2} \quad (A8)$$

If the head movement did not vary across trials ($\sigma_H^2 = 0$), then the square root of the sum $\sigma_h^2 + \sigma_i^2$ is the slope of the best-fitting cumulative Gaussian. The precision of the nonimage signal (σ_h) could then be obtained by measuring σ_i^2 in *phase 2* and subtracting it from the sum. However, $\sigma_H^2 \neq 0$. Variable head movements make the recovery of σ_h more complicated because they act as an external source of noise that varies with motion gain across the psychometric function.

Figure A1 shows that fitting a single cumulative Gaussian is an approximation at best. The black curves show example psychometric functions based on the formulae aforementioned (see legend for parameter values) whereas the red curves show the best-fitting single cumulative Gaussian. The difference between the two panels is whether a lapse-rate is included or not. The external noise has following two

effects: *1*) the asymptotes of the psychometric function move away from $P = 0$ and 1; *2*) the slope becomes steeper and is not well fit by a single cumulative Gaussian. The degree to which the external noise causes substantial departures from the standard fit depends on the relationship between the values of μ_H, σ_H^2, σ_h^2, σ_i^2, b and whether lapse-rate is allowed to vary in the standard fit.

FITTING PROCEDURE

We fit psychometric functions to our data based on the formulae aforementioned, using the measured head movements to estimate the mean and standard deviation of H. A matlab function for doing this can be found at https://doi.org/10.17605/OSF.IO/QCZ7W ("fitSMmodel"). *Phase 2* data were fit first, with σ_i^2 and λ free to vary, and μ_H and σ_H^2 fixed. The latter two parameters were based on the Gaussian distribution fit to the histograms of head movement speeds (see Fig. 3*B* in the main text for an example). *Phase 1* was then fit, with σ_H^2, b, and λ free to vary and σ_H^2, μ_H, and σ_H^2 fixed. To avoid local minima in the fit, each parameter was cycled through a search space of 20 values and the best fit chosen. This yielded 20^n separate cycles of the fitting routine, where n is the number of free parameters that was different for the two phases.

We did not find much difference between fitting the new psychometric function and fitting a single cumulative Gaussian. One likely explanation for this similarity was that the head movements were relatively consistent (σ_H^2 low) given the repetitive nature of the task. It may also be the case that including a constrained lapse-rate parameter soaked up a proportion of the asymptotic effect of the external noise. This can be seen by comparing Fig. A1*A* (no lapse rate) with Fig. A1*B* (constrained lapse rate $\leq$6%). The lapse rate mimics the asymptotic behavior produced by the external noise.

REGION-OF-INTEREST FOR CALCULATING HEAD ROTATION SPEED

The analysis depends on mean and variance of the head movements made in *interval 1* (see *Eqs. A7* and *A8*). The mean and variance were estimated from histograms of average speeds in the third sweep as described in the main text. To determine the region-of-interest (ROI), we compared the goodness-of-fit of psychometric functions from three ROIs: 20–80%, 20–60% or 40–60% of the sweep length. The psychometric functions were fit using maximum likelihood estimation, so the appropriate measure of goodness-of-fit is the deviance (38). Figure A2*A* shows that deviance in *experiment 1* did not change with the different ROIs used (the deviance has been averaged across conditions, phases, and participants). The same was true for *experiment 2* (not shown). However, Fig. A2*B* shows that an ROI of 20–80% produced a slower estimate of head movement speed than the other two ROIs, which was also more variable due to the inclusion of salient periods of acceleration and deceleration. Again the same was true for *experiment 2* (not shown). We therefore opted for an ROI of 20–60%.

DATA AVAILABILITY

The code used for fitting the model and analyzing the eye movements can be found here at https://doi.org/10.17605/OSF.IO/QCZ7W. The link also contains raw psychophysical and head movement data, together with summaries. Eye movement data can be made available on request.

ACKNOWLEDGMENTS

We thank the anonymous reviewers for the improvements suggested to the paper.

GRANTS

The work here was supported by a Leverhulme Trust Project Grant RPG-2018-151.

DISCLOSURES

No conflicts of interest, financial or otherwise, are declared by the authors.

AUTHOR CONTRIBUTIONS

J.D.H., M.G., J.F.C., and T.C.A.F. conceived and designed research; J.D.H., J.F.C., and T.C.A.F. performed experiments; J.D.H. and T.C.A.F. analyzed data; J.D.H., M.G., J.F.C., and T.C.A.F. interpreted results of experiments; J.D.H. and T.C.A.F. prepared figures; J.D.H. and T.C.A.F. drafted manuscript; J.D.H., M.G., J.F.C., and T.C.A.F. edited and

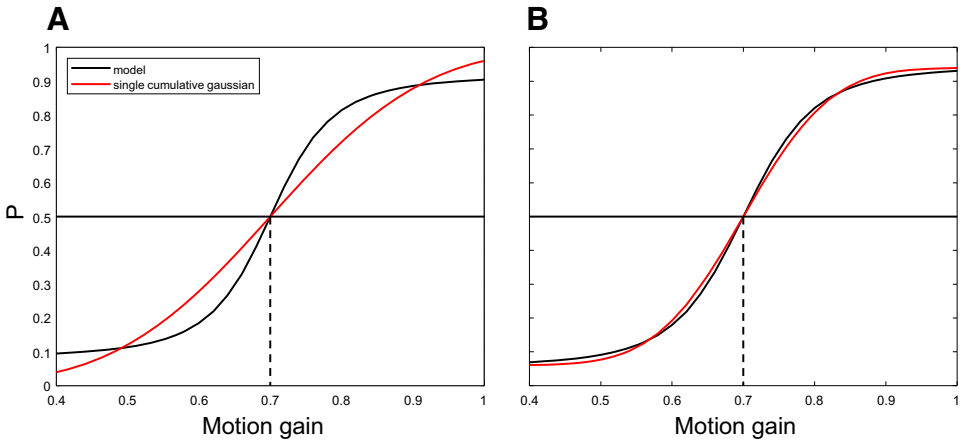

Figure A1. *A*: the black curve shows a psychometric function based on the gain-dependent noise model described in the text with $[\mu_H, \sigma_H^2, \sigma_h^2, \sigma_i^2, b, \lambda] = [20, 100, 2, 1, 0.7, 0]$. The red curve is the best-fitting cumulative Gaussian as determined by the Palamedes toolbox, with lapse rate $\lambda = 0$. *B*: same curves but with lapse-rate $\lambda = 0.06$ for the gain-dependent noise psychometric function, and free to vary for the single cumulative Gaussian [$\lambda \leq 0.06$, a standard constraint suggested by Wichmann and Hill (38)].

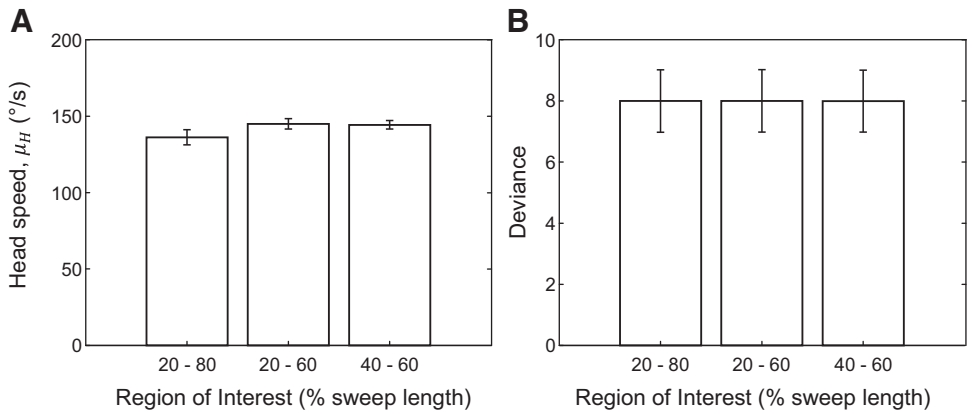

Figure A2. Head speed (*A*) and model goodness-of-fit (*B*) for each region-of-interest (ROI) used to analyze the head movements in *experiment 1*. Error bars are ±1SE.

revised manuscript; J.D.H., M.G., J.F.C., and T.C.A.F. approved final version of manuscript.

REFERENCES

1. **Clemens IAH**, **Selen LP**, **Pomante A**, **MacNeilage PR**, **Medendorp WP.** Eye movements in darkness modulate self-motion perception. *ENeuro* 4: ENEURO.0211-16.2016, 2017. doi:10.1523/ENEURO.0211-16.2016.
2. **Genzel D**, **Firzlaff U**, **Wiegrebe L**, **MacNeilage PR.** Dependence of auditory spatial updating on vestibular, proprioceptive, and efference copy signals. *J Neurophysiol* 116: 765–775, 2016. doi:10.1152/jn.00052.2016.
3. **Middlebrooks J**, **Green D.** Sound localization by human listeners. *Annu Rev Psychol* 42: 135–159, 1991. doi:10.1146/annurev.ps.42.020191.001031.
4. **Mallery RM**, **Olomu OU**, **Uchanski RM**, **Militchin VA**, **Hullar TE.** Human discrimination of rotational velocities. *Exp Brain Res* 204: 11–20, 2010. doi:10.1007/s00221-010-2288-1.
5. **Altman J**, **Viskov O.** Discrimination of perceived movement velocity for fused auditory image in dichotic stimulation. *J Acoust Soc Am* 61: 816–819, 1977. doi:10.1121/1.381371.
6. **De Bruyn B**, **Orban GA.** Human velocity and direction discrimination measured with random dot patterns. *Vision Res* 28: 1323–1335, 1988. doi:10.1016/0042-6989(88)90064-8.
7. **Brooks JX**, **Cullen KE.** Predictive sensing: the role of motor signals in sensory processing. *Biol Psychiatry Cogn Neurosci Neuroimaging* 4: 842–850, 2019. doi:10.1016/j.bpsc.2019.06.003.
8. **Skavenski AA.** Inflow as a source of extraretinal eye position information. *Vision Res* 12: 221–229, 1972. doi:10.1016/0042-6989(72)90113-7.
9. **Merton P.** Human position sense and sense of effort. *Symp Soc Exp Biol* 18: 387–400, 1964.
10. **von Holst E.** Relations between the central nervous system and the peripheral organs. *Br J Anim Behav* 2: 89–94, 1954. doi:10.1016/S0950-5601(54)80044-X.
11. **Tuthill JC**, **Azim E.** Proprioception. *Curr Biol* 28: R194–R203, 2018. doi:10.1016/j.cub.2018.01.064.
12. **St George RJ**, **Fitzpatrick RC.** The sense of self-motion, orientation and balance explored by vestibular stimulation. *J Physiol* 589: 807–813, 2011. doi:10.1113/jphysiol.2010.197665.
13. **Cullen KE**, **Zobeiri OA.** Proprioception and the predictive sensing of active self-motion. *Curr Opin Physiol* 20: 29–38, 2021. doi:10.1016/j.cophys.2020.12.001.
14. **Israël I**, **Warren WH.** Vestibular, proprioceptive, and visual influences on the perception of orientation and self-motion in humans. In: *Head Direction Cells and the Neural Mechanisms of Spatial Orientation*, edited by Weiner SI, Taube JS**.** Cambridge, MA: The MIT Press. 2005, p. 347–381.
15. **Angelaki DE**, **Cullen KE.** Vestibular system: the many facets of a multimodal sense. *Annu Rev Neurosci* 31: 125–150, 2008. doi:10.1146/annurev.neuro.31.060407.125555.
16. **Jörges B**, **Harris LR.** Object speed perception during lateral visual self-motion. *Atten Percept Psychophys* 84: 25–46, 2022. doi:10.3758/s13414-021-02372-4.
17. **Warren PA**, **Rushton SK.** Optic flow processing for the assessment of object movement during ego movement. *Curr Biol* 19: 1555–1560, 2009. doi:10.1016/j.cub.2009.07.057.
18. **Warren WH Jr**, **Hannon DJ.** Direction of self-motion is perceived from optical flow. *Nature* 336: 162–163, 1988. doi:10.1038/336162a0.
19. **Royden CS**, **Banks MS**, **Crowell JA.** The perception of heading during eye movements. *Nature* 360: 583–585, 1992. doi:10.1038/360583a0.
20. **Bedell HE**, **Klopfenstein JF**, **Yuan N.** Extraretinal information about eye position during involuntary eye movement: optokinetic afternystagmus. *Percept Psychophys* 46: 579–586, 1989. doi:10.3758/bf03208155.
21. **Barnes G.** Head-eye co-ordination: visual and nonvisual mechanisms of vestibulo-ocular reflex slow-phase modification. *Prog Brain Res* 76: 319–328, 1988. doi:10.1016/s0079-6123(08)64519-7.
22. **Clark B**, **Graybiel A.** The effect of angular acceleration on sound localization: the audiogyral illusion. *J Psychol* 28: 235–244, 1949. doi:10.1080/00223980.1949.9916005.
23. **Graybiel A**, **Hupp DI.** The oculo-gyral illusion; a form of apparent motion which may be observed following stimulation of the semicircular canals. *J Aviat Med* 17: 3–27, 1946.
24. **Carriot J**, **Bryan A**, **DiZio P**, **Lackner J.** The oculogyral illusion: retinal and oculomotor factors. *Exp Brain Res* 209: 415–423, 2011. doi:10.1007/s00221-011-2567-5.
25. **Freeman TC**, **Cucu MO**, **Smith L.** A preference for visual speed during smooth pursuit eye movement. *J Exp Psychol Hum Percept Perform* 44: 1629–1636, 2018. doi:10.1037/xhp0000551.
26. **Reisbeck TE**, **Gegenfurtner KR.** Velocity tuned mechanisms in human motion processing. *Vision Res* 39: 3267–3285, 1999. doi:10.1016/s0042-6989(99)00017-6.
27. **Freeman TC**, **Leung J**, **Wufong E**, **Orchard-Mills E**, **Carlile S**, **Alais D.** Discrimination contours for moving sounds reveal duration and distance cues dominate auditory speed perception. *PLoS One* 9: e102864, 2014. doi:10.1371/journal.pone.0102864.
28. **Carlile S**, **Best V.** Discrimination of sound source velocity in human listeners. *J Acoust Soc Am* 111: 1026–1035, 2002. doi:10.1121/1.1436067.
29. **Aubert H.** Die Bewegungsempfindung: Zweite Mittheilung. *Pflugers Arch* 40: 459–480, 1887. doi:10.1007/BF01612710.
30. **Fleischl EV.** Physiologisch-optische Notizen [Physiological-optical notes], 2. Mitteilung. *Sitzung Wiener Bereich der Akademie der Wissenschaften* 3: 7, 1882.
31. **Garzorz IT**, **Freeman TC**, **Ernst MO**, **MacNeilage PR.** Insufficient compensation for self-motion during perception of object speed: the vestibular Aubert-Fleischl phenomenon. *J Vis* 18: 9, 2018. doi:10.1167/18.13.9.
32. **Moscatelli A**, **Scotto CR**, **Ernst MO.** Illusory changes in the perceived speed of motion derived from proprioception and touch. *J Neurophysiol* 122: 1555–1565, 2019. doi:10.1152/jn.00719.2018.
33. **Freeman TC**, **Culling JF**, **Akeroyd MA**, **Brimijoin WO.** Auditory compensation for head rotation is incomplete. *J Exp Psychol Hum Percept Perform* 43: 371–380, 2017. doi:10.1037/xhp0000321.

34. **Stevenson-Hoare JO**, **Freeman TC**, **Culling JF.** The pinna enhances angular discrimination in the frontal hemifield. *J Acoust Soc Am* 152: 2140–2149, 2022. doi:10.1121/10.0014599.
35. **Prins N**, **Kingdom FA.** Applying the model-comparison approach to test specific research hypotheses in psychophysical research using the Palamedes toolbox. *Front Psychol* 9: 1250, 2018. doi:10.3389/fpsyg.2018.01250.
36. **Serafin S**, **Nilsson NC**, **Sikstrom E**, **De Goetzen A**, **Nordahl R.** Estimation of detection thresholds for acoustic based redirected walking techniques. *2013 IEEE Virtual Reality (VR)*. Lake Buena Vista, FL, 2013, p. 161–162. doi:10.1109/VR.2013.6549412.
37. **Steinicke F**, **Bruder G**, **Jerald J**, **Frenz H**, **Lappe M.** Estimation of detection thresholds for redirected walking techniques. *IEEE Trans Vis Comput Graph* 16: 17–27, 2010. doi:10.1109/TVCG.2009.62.
38. **Wichmann FA**, **Hill NJ.** The psychometric function. I. Fitting, sampling, and goodness of fit. *Percept Psychophys* 63: 1293–1313, 2001. doi:10.3758/bf03194544.
39. **Nilsson NC**, **Peck T**, **Bruder G**, **Hodgson E**, **Serafin S**, **Whitton M**, **Steinicke F**, **Rosenberg ES.** 15 years of research on redirected walking in immersive virtual environments. *IEEE Comput Graph Appl* 38: 44–56, 2018. doi:10.1109/MCG.2018.111125628.
40. **Cherni H**, **Métayer N**, **Souliman N.** Literature review of locomotion techniques in virtual reality. *Int J Virtual Reality* 20: 1–20, 2020. doi:10.20870/IJVR.2020.20.1.3183.
41. **Halow S**, **Liu J**, **Folmer E**, **MacNeilage PR.** Motor signals mediate stationarity perception. *Multisens Res* 36: 703–724, 2023. doi:10.1163/22134808-bja10111.
42. **Wyatt HJ.** Detecting saccades with jerk. *Vision Res* 38: 2147–2153, 1998. doi:10.1016/s0042-6989(97)00410-0.
43. **Leigh RJ**, **Zee DS** (Editors)**.** *The Neurology of Eye Movements* (3rd ed.). Oxford, UK: Oxford University Press, 1999. (Contemporary Neurology Series).
44. **Laming D.** Weber's law. In: *Inside Psychology: A Science over 50 Years*, edited by Rabbitt P. Oxford, UK: Oxford University Press, 2009, p. 177–189.
45. **Freeman TC**, **Champion RA**, **Warren PA.** A Bayesian model of perceived head-centered velocity during smooth pursuit eye movement. *Curr Biol* 20: 757–762, 2010. doi:10.1016/j.cub.2010.02.059.
46. **Powell G**, **Meredith Z**, **McMillin R**, **Freeman TC.** Bayesian models of individual differences: combining autistic traits and sensory thresholds to predict motion perception. *Psychol Sci* 27: 1562–1572, 2016. doi:10.1177/0956797616665351.
47. **Harrison JJ**, **Freeman TC**, **Sumner P.** Saccadic compensation for reflexive optokinetic nystagmus just as good as compensation for volitional pursuit. *J Vis* 15: 15.1.24, 2015. doi:10.1167/15.1.24.
48. **Bentvelzen A**, **Leung J**, **Alais D.** Discriminating audiovisual speed: optimal integration of speed defaults to probability summation when component reliabilities diverge. *Perception* 38: 966–987, 2009. doi:10.1068/p6261.
49. **Rideaux R**, **Welchman AE.** But still it moves: static image statistics underlie how we see motion. *J Neurosci* 40: 2538–2552, 2020. doi:10.1523/JNEUROSCI.2760-19.2020.
50. **Furman M**, **Gur M.** And yet it moves: perceptual illusions and neural mechanisms of pursuit compensation during smooth pursuit eye movements. *Neurosci Biobehav Rev* 36: 143–151, 2012. doi:10.1016/j.neubiorev.2011.05.005.
51. **Rabbitt RD.** Semicircular canal biomechanics in health and disease. *J Neurophysiol* 121: 732–755, 2019. doi:10.1152/jn.00708.2018.
52. **Cullen KE.** Vestibular processing during natural self-motion: implications for perception and action. *Nat Rev Neurosci* 20: 346–363, 2019. doi:10.1038/s41583-019-0153-1.
53. **Prsa M**, **Gale S**, **Blanke O.** Self-motion leads to mandatory cue fusion across sensory modalities. *J Neurophysiol* 108: 2282–2291, 2012. doi:10.1152/jn.00439.2012.
54. **Hillis JM**, **Watt SJ**, **Landy MS**, **Banks MS.** Slant from texture and disparity cues: optimal cue combination. *J Vis* 4: 967–992, 2004. doi:10.1167/4.12.1.
55. **Nouri S**, **Karmali F.** Variability in the vestibulo-ocular reflex and vestibular perception. *Neuroscience* 393: 350–365, 2018. doi:10.1016/j.neuroscience.2018.08.025.
56. **Weiss Y**, **Simoncelli EP**, **Adelson EH.** Motion illusions as optimal percepts. *Nat Neurosci* 5: 598–604, 2002. doi:10.1038/nn0602-858.
57. **Stocker AA**, **Simoncelli EP.** Noise characteristics and prior expectations in human visual speed perception. *Nat Neurosci* 9: 578–585, 2006. doi:10.1038/nn1669.
58. **Senna I**, **Parise CV**, **Ernst MO.** Hearing in slow-motion: humans underestimate the speed of moving sounds. *Sci Rep* 5: 14054, 2015. doi:10.1038/srep14054.
59. **Thompson P**, **Brooks K**, **Hammett ST.** Speed can go up as well as down at low contrast: Implications for models of motion perception. *Vision Res* 46: 782–786, 2006. doi:10.1016/j.visres.2005.08.005.
60. **Hassan O**, **Hammett ST.** Perceptual biases are inconsistent with Bayesian encoding of speed in the human visual system. *J Vis* 15: 9, 2015. doi:10.1167/15.2.9.
61. **Hammett ST**, **Champion RA**, **Thompson PG**, **Morland AB.** Perceptual distortions of speed at low luminance: evidence inconsistent with a Bayesian account of speed encoding. *Vision Res* 47: 564–568, 2007. doi:10.1016/j.visres.2006.08.013.
62. **Freeman TC**, **Powell G.** Perceived speed at low luminance: lights out for the Bayesian observer? *Vision Res* 201: 108124, 2022. doi:10.1016/j.visres.2022.108124.
63. **Jones PR.** A tutorial on cue combination and Signal Detection Theory: using changes in sensitivity to evaluate how observers integrate sensory information. *J Math Psychol* 73: 117–139, 2016. doi:10.1016/j.jmp.2016.04.006.